



Article

Nanoparticle Behaviour in an Urban Street Canyon at Different Heights and Implications on Indoor Respiratory Doses

Maurizio Manigrasso ^{1,*}, Carmela Protano ², Matteo Vitali ²  and Pasquale Avino ³ ¹ Department of Technological Innovations, INAIL, 00143 Rome, Italy² Department of Public Health and Infectious Diseases, Sapienza University of Rome, 00185 Rome, Italy; carmela.protano@uniroma1.it (C.P.); matteo.vitali@uniroma1.it (M.V.)³ Department of Agricultural, Environmental and Food Sciences (DiAAA), University of Molise, 86100 Campobasso, Italy; avino@unimol.it

* Correspondence: m.manigrasso@inail.it

Received: 23 September 2019; Accepted: 29 November 2019; Published: 3 December 2019



Abstract: The amount of outdoor particles that indoor environments receive depends on the particle infiltration factors (F_{in}), peculiar of each environment, and on the outdoor aerosol concentrations and size distributions. The respiratory doses received, while residing indoor, will change accordingly. This study aims to ascertain to what extent such doses are affected by the vertical distance from the traffic sources. Particle number size distributions have been simultaneously measured at street level and at about 20 m height in a street canyon in downtown Rome. The same F_{in} have been adopted to estimate indoor aerosol concentrations, due to the infiltration of outdoor particles and then the relevant daily respiratory doses. Aerosol concentrations at ground floor were more than double than at 20 m height and richer in ultrafine particles. Thus, although aerosol infiltration efficiency was on average higher at 20 m height than at ground floor, particles more abundantly infiltrated at ground level. On a daily basis, this involved a 2.5-fold higher dose at ground level than at 20 m height. At both levels, such doses were greater than those estimated over the period of activity of some indoor aerosol sources; therefore, they represent an important contribution to the total daily dose.

Keywords: ultrafine particles; aerosol; urban street canyon; outdoor pollution; indoor air quality; respiratory doses; MPPD

1. Introduction

Outdoor and indoor air quality is a major determinant of human health. Indeed, the World Health Organization estimated that air pollution kills seven million people worldwide every year and nine out of ten individuals are exposed to high concentrations of airborne pollutants [1]. Particulate matter (PM) is one of the most relevant air pollutants, linked to the pathogenesis of several human diseases involving numerous systems and apparatuses. In particular, many studies highlighted that some specific PM fractions (particles diameter $\leq 10 \mu\text{m}$ and $\leq 2.5 \mu\text{m}$, defined respectively as PM_{10} and $\text{PM}_{2.5}$) were associated to cardiovascular, respiratory and neurodegenerative diseases [2–4]. In addition, in 2015 PM in outdoor air was classified as a Group 1 carcinogen to humans by the International Agency for Research on Cancer (IARC) [5]. Over the last years, researchers focused their attention on smaller particles, specifically on ultrafine particles (UFPs, that is particles with sizes $\leq 100 \text{ nm}$); indeed, particles $> 2.5 \mu\text{m}$ are removed quickly (few hours) from the atmosphere due to dry and wet deposition, whereas particles $< 1 \mu\text{m}$ persist for longer times and easily contaminate both outdoor and indoor air [6–8] and/or are transported over long ranges. Besides, UFPs have a high number

concentration, very high surface area and surface area reactivity, as well as small size compared to the dimensions of cellular structures. These characteristics allow them a great ability to absorb organic molecules and penetrate into cellular targets [9,10]. For such reasons, both number concentration and surface area metrics have been suggested to explain their biological effects better than the traditional mass metric. Recent studies reported that UFPs are more toxic in comparison with larger particles and induce adverse effects on respiratory and cardiovascular systems via intracellular oxidative stress activation and inflammation response [11]. Besides, UFPs can pass directly in brain tissue through the olfactory bulb and increase the risk of developing neurodegenerative diseases, in particular Alzheimer's disease [12]. Adverse outcomes on children's health associated with UFP exposure also have been recently reported, especially among children with respiratory diseases [13]. Such adverse effects on human health are of particular concern, considering that UFPs are released in high concentrations from many anthropogenic sources both outdoor and in many occupational and domestic scenarios [14]. Vehicular traffic is the main source of UFPs in urban areas [15–18]. About 70–90% of particle number concentration in urban areas is due to UFPs [19,20]. However, in spite of the wide consensus on their detrimental effects on human health, PM air quality limits and consequently air monitoring networks rely on mass metrics, which poorly represents UFP concentration. Moreover, specific building and road layouts may hinder pollutant dispersion and worsen air quality. Therefore, there is an important need to focalize studies on this class of particles and to address specific environments, such as urban street canyons, that represent situations of increased population respiratory exposure. In indoor settings, UFPs are released by devices and appliances commonly used (conventional and electronic cigarettes, electric appliances, etc.) or activities usually practiced (cooking) [21–26].

In the last years more attention was given to indoor air quality, because a great part of the general population spends most of the time (>90%) in enclosed environments [27] and indoor air may be of worse quality than outdoor, since indoor air pollutants are the sum of those penetrated from outdoors and those directly produced indoors [28,29]. On this point, several studies [30–32] have addressed the issue of vertical profiles of particle concentrations in urban areas and have highlighted their relevance in terms of indoor air quality. However, to date, studies describing how the different vertical aerosol concentrations and size distributions affect the aerosol doses received by the respiratory system of individuals residing in the same building but at different heights are lacking. Thus, the aim of the present study was to ascertain to what extent such doses are affected by the vertical distance from the street level.

2. Experiments

2.1. Aerosol Measurements

Atmospheric particle number–size distributions were simultaneously measured by means of two TSI Fast Mobility Particle Sizer spectrometers (model 3091, FMPS, Shoreview, MN, USA) equipped at their inlets with a cyclone with a 1 μm 50% cut-point. The instruments were located at the ground level and at 20 m height in a building in downtown Rome during the winter season. The site (41°53'46" N, 12°29'46" E) was in a narrow double lane street (street width, W , of about 8 m), with high buildings on both sides (average height, H , of about 25 m). Such a street can be considered a street canyon, as the aspect ratio H/W is about 3:1. By using a camera, the number of vehicles (cars, buses, and motorcycles) circulating per unit of time was evaluated on average to be about 18 vehicles min^{-1} .

FMPS counts and classifies particles, according to their electrical mobility, in 32 size channels, in the range 5.6–560 nm, with 1 s time resolution. It operates at a high flow rate (10 L min^{-1}) to minimize diffusion losses of UFPs and at ambient pressure, to prevent evaporation of volatile and semi-volatile particles [33]. The performance of the FMPS was investigated by Jeong et al. [34] by comparison with a Scanning Mobility Particle Sizer (SMPS). The authors evaluated that the SMPS number concentration, in the size range from 6 nm to 100 nm, is about 34% lower than the FMPS measurements, due to the diffusion losses of particles in the SMPS. The diffusion loss corrected SMPS number concentration is on average about 15% higher than the FMPS data. One-day outdoor aerosol measurements were

selected to calculate the indoor aerosol concentrations inside the building at the ground floor and at the 5th floor (20 m height) utilizing the size-resolved average infiltration factors (F_{in}) measured by Bennett and Koutrakis [35]. The average F_{in} estimated by these authors were based on time-dependent aerosol concentrations (0.02–4 μm size range) and air-exchange rate (in the range of about 0.5–1.5 h^{-1}) measurements carried out in nine homes with a sampling duration ranging from 6 to 12 consecutive days. The F_{in} relative to the FMPS size class were estimated by interpolation with a cubic spline [36] (Figure S1 of Supplementary Material). For aerodynamic diameters (0.01–0.02 μm) outside the Bennett and Koutrakis [35] measurement range, the F_{in} value of 0.02 μm particles was adopted. We decided to rely on outdoor rather than on indoor aerosol measurements in order to perform dosimetry estimates in the absence of indoor aerosol sources. Referring to two real indoor environments would have made it difficult to isolate the effect of the outdoor aerosol concentration gradient on the indoor respiratory doses, due to the different air ventilation and possibly occurring aerosol generation events.

Throughout the aerosol measurements, atmospheric pressure, temperature, relative humidity, wind speed, and wind direction were continuously measured with 5 min averaging time (Figure S2 of Supplementary Material).

2.2. Aerosol Dosimetry

To estimate aerosol doses due to the infiltration of outdoor aerosols into indoor environments, a 22 h daily indoor residence was considered, as reported by Hussein [37]. Three time periods (t_r) were assumed according to the different work and physical activities: 7 h sleeping (from 11 p.m. to 6 a.m.), three hours sitting awake (6–7 a.m. and 9–11 p.m.), 12 h light work (8 a.m.–4 p.m. and 5 p.m.–9 p.m.). The particle regional deposition fractions ($F^R(d_{ai})$) as a function of aerodynamic diameter (d_{ai}) have been estimated using the Multiple-Path Particle model Dosimetry (MPPD v3.01, ARA 2015, ARA, Arlington, VA, USA) [38]. The 60th percentile human stochastic lung was considered along with the following settings: (i) a uniformly expanding flow, (ii) an upright or a lying on back (for the sleeping period) body orientation, and (iii) a nasal breathing with a 0.5 inspiratory fraction and no pause fraction. Moreover, the following parameters were used for a Caucasian adult male, based on the ICRP report [39]: (i) a functional residual capacity (FRC) of 3300 mL, (ii) an upper respiratory tract (URT) volume equal to 50 mL, (iii) a breathing frequency of 12 min^{-1} for sleeping and sitting awake activity and 20 min^{-1} for light work activity, and (iv) an air volume inhaled during a single breath (tidal volume, V_t) of 0.625 L, 0.750 L, and 1.25 L for sleeping, sitting awake, and light work activities, respectively. In particular, the breathing frequencies adopted for sitting awake and light work activities, if multiplied by the tidal volume adopted in the present study, give minute ventilation values similar to those reported by Hussein et al. [40] for sitting and walking activities, respectively.

Since FMPS measures aerosol size number distribution as a function of the electrical mobility diameter (d_m), d_m values have been transformed to aerodynamic diameter (d_a) according to Equation (1) [41]:

$$d_a = d_m \sqrt{\frac{1}{\chi} \times \frac{\rho \times C_c(d_m)}{\rho_0 C_c(d_a)}}, \quad (1)$$

where C_c is the Cunningham slip factor for a given diameter, ρ is the particle density (1.5 g cm^{-3} density was assumed) [42,43], ρ_0 is the standard density (1 g cm^{-3}), and χ is the particle dynamic shape factor. χ as a function of aerodynamic diameter was estimated by interpolating with a cubic spline the data reported by Hu et al. [44] in the range from 0.1 to 1.8 μm in Beijing. For d_a below this range the relevant lower bound χ value was adopted (1.13 for $d_a < 0.1 \mu\text{m}$).

Aerosol number doses $D^R(d_{ai}, t)$ deposited in the head (H), tracheobronchial (TB), and alveolar (Al) regions, as functions of time (t) and of the aerodynamic diameter (d_{ai}), were estimated according to Equation (2):

$$D^R(d_{ai}, t) = F_{in} \times C(d_{ai}, t) \times F^R(d_{ai}) \times V_t \quad R = \text{H, TB, Al}, \quad (2)$$

where $C(d_{ai}, t)$ is the average aerosol concentration over a single inspiratory act as a function of time and of aerodynamic diameter. Particle hygroscopic growth was not accounted for in the calculations.

Total regional aerosol doses have been estimated according to Equation (3), where the summation is carried out over the FMPS size classes:

$$D_{Tot}^R(t) = \sum_i D^R(d_{ai}, t) \quad R = H, TB, Al. \quad (3)$$

Total aerosol doses deposited into the respiratory system has been calculated according to Equation (4):

$$D_{Tot}^{Tot}(t) = D_{Tot}^H(t) + D_{Tot}^{TB}(t) + D_{Tot}^{Al}(t). \quad (4)$$

Cumulative regional and total doses over a given residence time (t_r) have been calculated according to Equations (5) and (6):

$$D_{Tot}^R(t_r) = \sum_{t=0}^{t_r} D_{Tot}^R(t) \quad R = H, TB, Al, \quad (5)$$

$$D_{Tot}^{Tot}(t_r) = \sum_{t=0}^{t_r} D_{Tot}^{Tot}(t). \quad (6)$$

The cumulative regional ($D_{Tot}^R(t_{day})$) and total daily dose ($D_{Tot}^{Tot}(t_{day})$) has been calculated as the sum of the $D_{Tot}^R(t_r)$ and $D_{Tot}^{Tot}(t_r)$ doses relative to the free time period (t_r) considered (7 h sleeping, 3 h sitting awake, 12 h light work, and $t_{day} = 22$ h).

The cumulative total dose size distribution over a given residence time ($D^{Tot}(d_{ai}, t_r)$) has been calculated according to Equation (7):

$$D^{Tot}(d_{ai}, t_r) = \sum_{t=0}^{t_r} D^H(d_{ai}, t) + D^{TB}(d_{ai}, t) + D^{Al}(d_{ai}, t). \quad (7)$$

3. Results and Discussion

3.1. Aerosol Measurements

Outdoor aerosol total number concentrations (C_{Tot}) over the 24 h considered were on average 2.3-fold higher at ground floor than at 20 m heights with concentration ratios, for individual spikes, exceeding 20, up to about 40. Both sets of data shared the same temporal modulation with two broad peaks centred at 8 a.m. and 7 p.m., determined by the daily traffic flow variation and by the planetary boundary layer (PBL) mixing height that was highest in the central part of the day during periods of high solar radiation (Figure 1) [45–47].

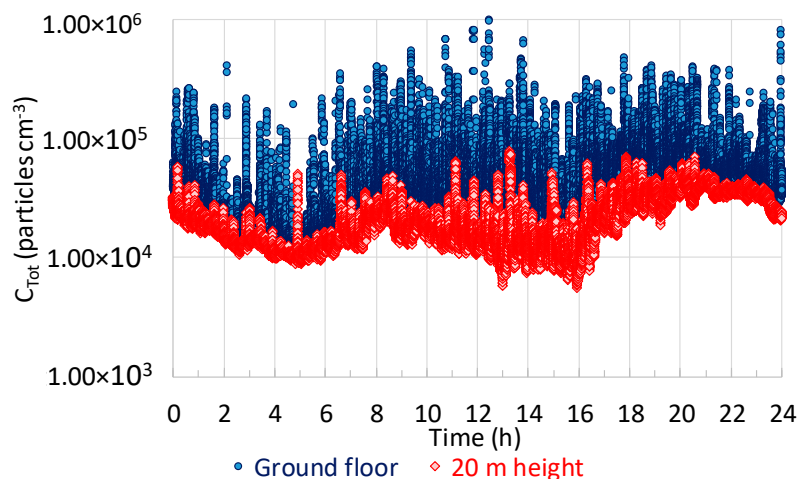


Figure 1. Total (5.6–560 nm electrical mobility diameter) aerosol concentrations measured with a 1 s time resolution at ground floor and at 20 m height in a street canyon in downtown Rome.

Spike concentrations were more intense and frequent at ground level than at 20 m heights due to the proximity of the vehicular exhausts. The contribution of UFPs at ground level was slightly higher than at 20 m height, on average respectively 88% and 84%, although at ground level it occasionally dropped below the relevant value at 20 m height (Figure 2). Such occurrence was probably due to the turbulence at ground level generated by the vehicular traffic, with consequent dust re-suspension and removal of smaller particles by impaction on coarse re-suspended particles.

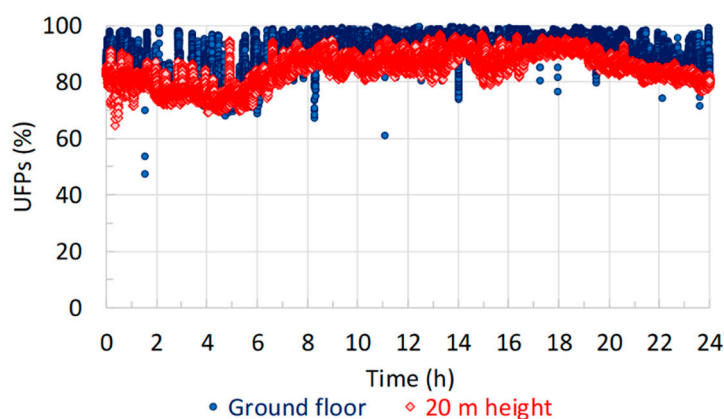


Figure 2. Temporal trend of ultrafine particle (UFP) % contribution at ground floor and at 20 m height in a street canyon in downtown Rome.

Small particle ($<0.1 \mu\text{m}$) deposition is efficient due to their Brownian diffusion, whereas interception, impaction, and gravitational settling are important deposition mechanism for larger particles ($>2 \mu\text{m}$) [48]. Minimum values of deposition velocities occur for particles in the range $0.1\text{--}2 \mu\text{m}$, because neither Brownian diffusion nor impaction or interception are effective mechanisms [48]. Consequently, nucleation particles are less persistent than larger-sized particles. Therefore, they are predominant during traffic hours when freshly formed from vehicular exhausts, but decrease significantly at night when traffic is less intense and particles in the accumulation mode predominate. Therefore, the geometric mean diameter (GMD), both at ground level and at 20 m height (Figure 3), follows a temporal trend characterized by low values during the day and increased values during nocturnal hours.

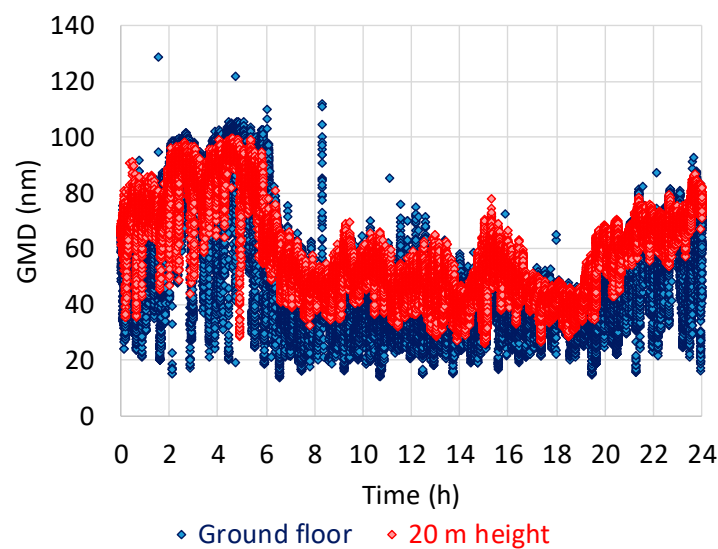


Figure 3. Temporal trend of the geometric mean aerodynamic diameter (GMD) at ground level and at 20 m height in a street canyon in downtown Rome.

For these reasons, and due to the higher distance from the traffic exhaust, as a general trend GMD is higher at 20 m height than at ground level, as shown in Figure 4, where the ratio of GMD at the two levels is plotted as a function of time. This feature involves some consequences in terms of aerosol capability of infiltrating indoor environments.

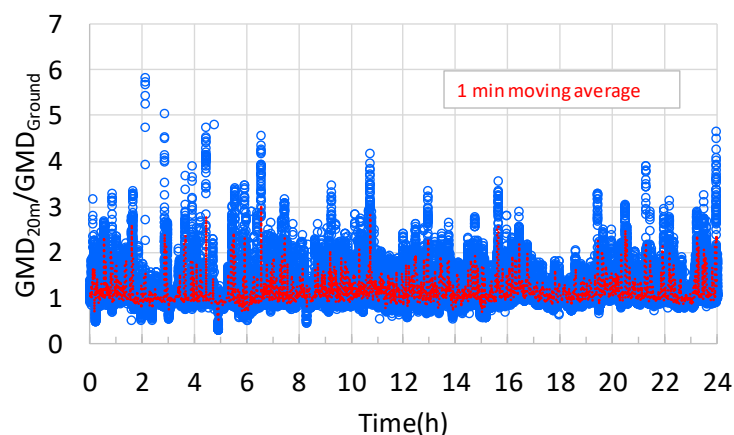


Figure 4. The ratio of geometric mean aerodynamic diameter (GMD) at 20 m height to GMD at ground level in a street canyon in downtown Rome.

To discuss this point, the infiltration factors pertaining to each GMD value have been calculated at both levels (Figure 5). Such a dataset, being characterized by highly frequent spike values, has been smoothened by calculating the relevant 1 h mobile averages ($F_{in}(GMD)$). The smoothened dataset so obtained allows to assess a general daily trend of the average infiltration factor (Figure 5). At both levels the $F_{in}(GMD)$ is higher during nocturnal hours than during daytime, in the same periods when a maximum is observed in the GMD temporal trends (Figure 3). Moreover, due to the higher GMD values, the aerosol infiltration efficiency at 20 m height is, on average, slightly higher than at ground level.

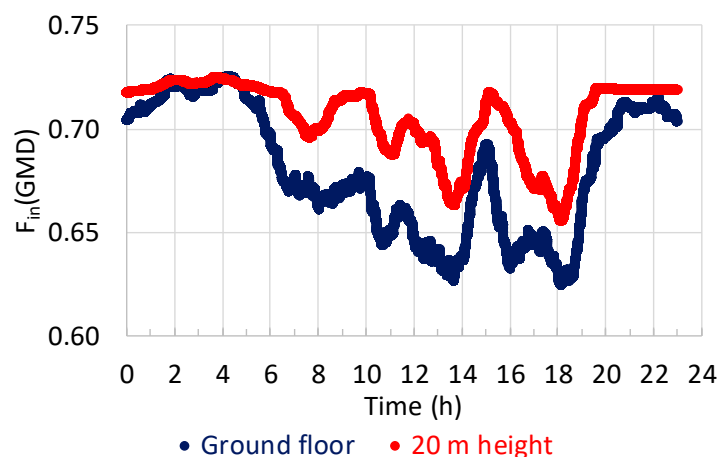


Figure 5. The 1 h moving average of the infiltration factors (F_{in}) calculated at the GMD values at ground level and at 20 m height.

This occurs because the infiltration efficiency for small particles ($<0.1 \mu m$) due to their efficient Brownian deposition is lower than for accumulation mode particles. The infiltration factors $F_{in}(GMD)$ plotted in Figure 5 are close to the upper limit of the literature F_{in} range for $PM_{2.5}$ discussed by Chen and Zhao [49]. This behaviour is coherent with the trend of F_{in} as a function of particle size reported in Figure S1 in the Supplementary Material, showing a maximum in the range $0.1\text{--}0.3 \mu m$ and a decreasing trend for greater aerodynamic diameters.

3.2. Aerosol Dosimetry

Figure 6 describes the cumulative regional ($D_{Tot}^R(t_r)$) and total dose ($D_{Tot}^{Tot}(t_r)$) estimated for indoor environments at ground floor and at 20 m height, in the absence of indoor aerosol emission sources. They represent the contribution due to the indoor infiltration of outdoor aerosol. These doses are about 2.6-, 1.7-, and 1.9-fold higher at ground floor than at 20 m height, respectively, for light work, sitting awake, and sleeping physical activities. Such differences are determined by the higher outdoor aerosol concentrations at the street level (Figure 1) that abundantly outweigh the higher average infiltration efficiency of the aerosol at 20 m height (Figure 5). The highest $D_{Tot}^{Tot}(t_r)$ doses have been estimated during the period of light work activity (1.16×10^{11} particles at 20 m height and 3.08×10^{11} particles at ground floor) and the lowest for sitting awake activity (1.34×10^{10} particles at 20 m height and 2.24×10^{10} particles at ground floor) because of both the longer time period and of the higher tidal volume and breathing frequency for light work activities.

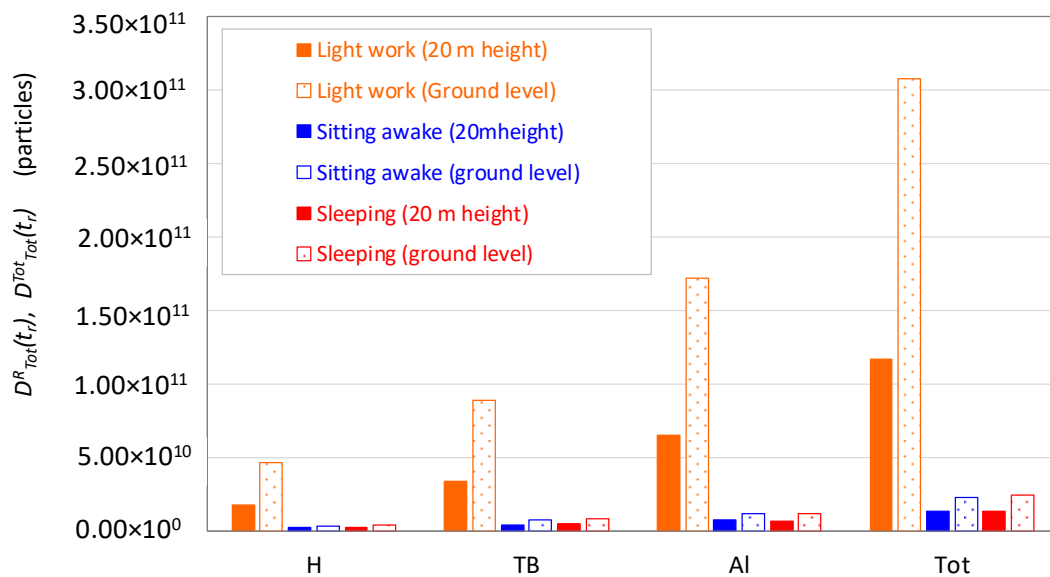


Figure 6. Cumulative regional ($D_{Tot}^R(t_r)$) and total ($D_{Tot}^{Tot}(t_r)$) aerosol doses over a residence time (t_r) of 7 h, 3 h, and 12 h, respectively, for sleeping, sitting awake, and light work activities, at ground level and at 20 m height.

The different work activities also affect the particle dose distribution within the respiratory system. The fraction of particles deposited in the H and TB regions decreases passing from sleeping (respectively 18% and 35% at ground level and 17% and 33% at 20 m height) to light work activity (respectively 15% and 29% at both levels); conversely, the AI fraction increases (from 47% and 50%, respectively, at ground level, and at 20 m height, to 56% at both levels).

Figure 7 shows the size distributions of $\dot{D}_{Tot}^R(t_r)$ doses per unit time at ground level and at 20 m height. For light work activity, at both levels, three modes of about the same importance were present at 0.012, 0.019, and 0.039 μm and a fourth one, less intense, at about 0.107 μm . The first two modes occurred also for the sitting awake and sleeping activities, but the more intense modes were at higher particle diameters (0.107 and 0.060 μm , respectively, at ground level and at 20 m height), reflecting the more abundant presence of Aitken and of accumulation mode particles during nocturnal hours.

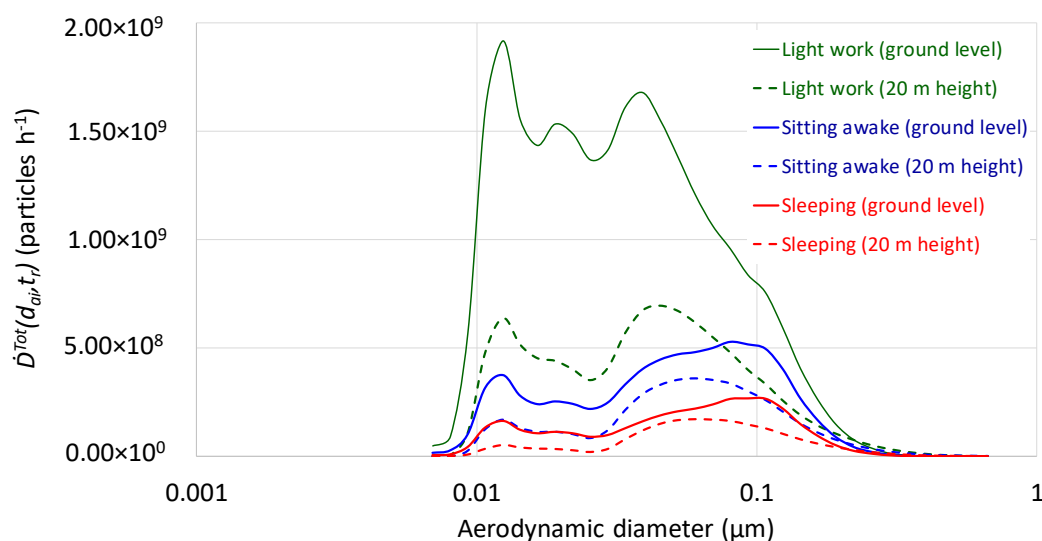


Figure 7. Cumulative total dose size distribution ($\dot{D}_{Tot}^{Tot}(d_{ai}, t_r)$) per unit time at ground level and at 20 m height, over a residence time (t_r) of 7 h, 3 h, and 12 h, respectively for sleeping, sitting awake, and light work activities.

Figure 8 describes the cumulative regional ($D_{Tot}^R(t_{day})$) and total ($D_{Tot}^{Tot}(t_{day})$) daily doses estimated for one day residence in an indoor environment at ground floor and at 20 m height. 3.55×10^{11} and 1.43×10^{11} particles are respectively deposited into the respiratory system at ground floor and at 20 m height. About 15%, 30%, and 55% of such doses are respectively deposited in the H, TB, and AI regions.

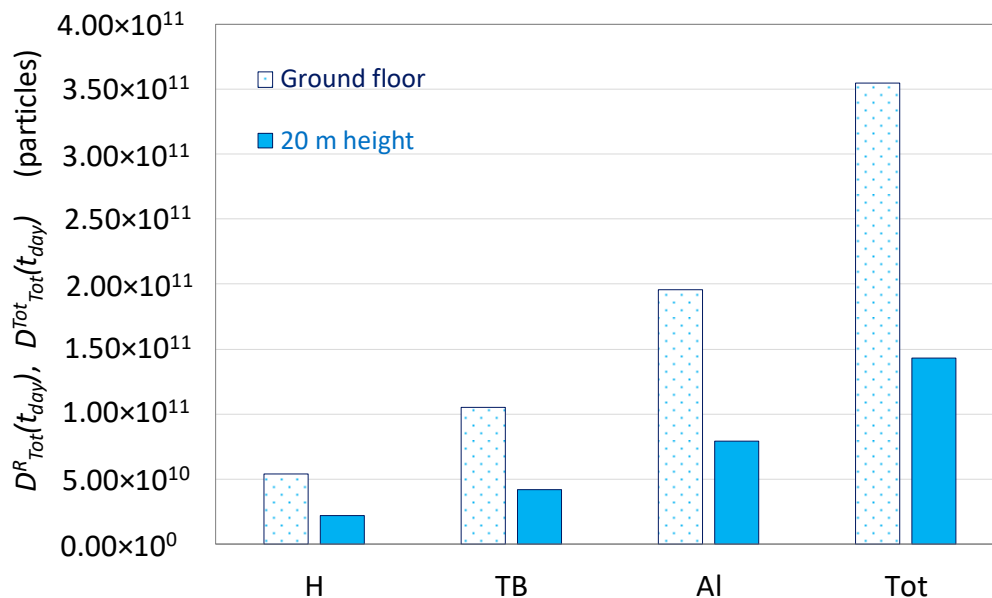


Figure 8. Cumulative regional ($D_{Tot}^R(t_{day})$) and total daily dose ($D_{Tot}^{Tot}(t_{day})$) at ground level and at 20 m height.

$D_{Tot}^{Tot}(t_{day})$ at both levels are compared in Figure 9a with the total particle doses deposited into the respiratory system after 1 h exposure time (t_{exp}), at the same site and in the same day, at outdoor aerosol during the traffic peak hour and after 1 h exposure to atmospheric aerosol in Mount Terminillo, a central Italy 2217 m high mount region ($D_{Tot}^{Tot}(t_{exp})$) [50]. In the same figure the comparison is carried out with the main combustion and non-combustion sources encountered in indoor environments [23–25], in this case t_{exp} represents the period of source operation (5, 1.5, 6, 5, 6, 6, 4, 4, and 5 min) respectively for hairdryer, electric drill, vacuum cleaner, hot flat iron, mosquito coil, incense cone, tobacco cigarette, e-cigarette, and meat grilling.

Due to the longer exposure time (22 h), at both levels $D_{Tot}^{Tot}(t_{day})$ are higher than the doses relative to all the other operations, with the exception of the meat grilling without exhaust ventilation. In that case, a single 5 min exposure is associated to a dose that is 1.7- and 4.2-fold higher than the cumulative total daily doses at ground floor and 20 m height (22 h exposure). To account for the different time scales, the doses of Figure 9a have been referred to unit exposure time ($\dot{D}_{Tot}^{Tot}(t_{day})$, $\dot{D}_c^{Tot}(t_{exp})$, $\dot{D}_{Tot}^{Tot}(t_{exp})$) and plotted in Figure 9b. On this basis, with the exception of the relatively low aerosol emitting first generation e-cigarette [23,25], all the doses due to indoor aerosol sources are higher than the doses due to the infiltration of outdoor particles.

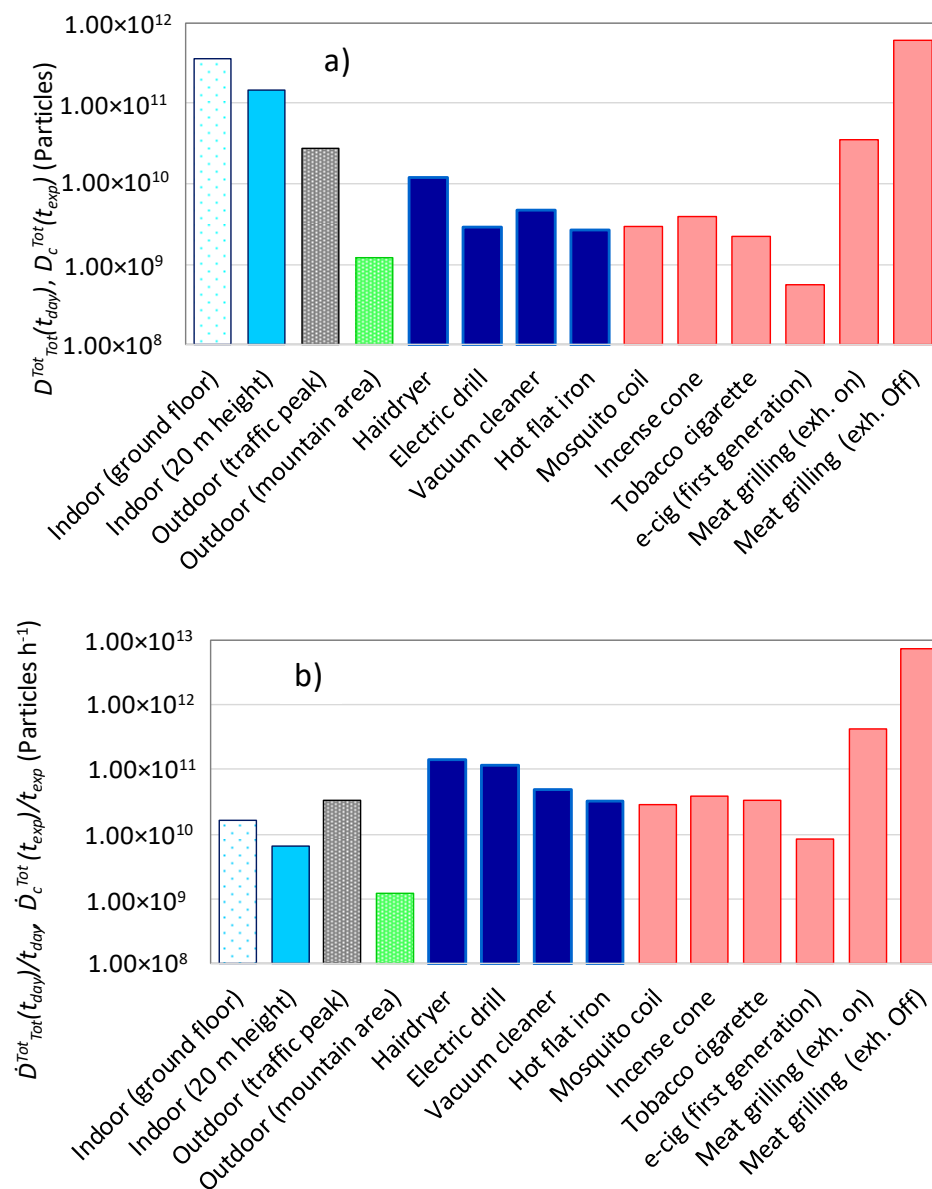


Figure 9. (a) $D_{Tot}^{Tot}(t_{day})$ at ground level and at 20 m height compared with the total particle doses deposited into the respiratory system ($D_{Tot}^{Tot}(t_{exp})$) after exposure to different indoor and outdoor aerosol sources for given exposure times (t_{exp}). (b) The same comparison is made for the relevant doses per unit exposure time ($\dot{D}_{Tot}^{Tot}(t_{day}), \dot{D}_{Tot}^{Tot}(t_{exp})$).

Moreover, the dose after 1 h outdoor exposure in the Terminillo mountain area emphasizes the influence of outdoor pollution on indoor air quality. Such dose is 13- and 5-fold lower than the 1 h doses relative, respectively, to the ground floor and to the 20 m height indoor environments in an urban street canyon.

4. Conclusions

Particle number size distributions have been simultaneously measured at street level and at about 20 m height, with 1 s time resolution, at a street canyon in downtown Rome. At both heights, the total particle number concentrations shared a temporal trend that on an hourly time scale was determined by the daily traffic flow variations and by the PBL modulation. On a few seconds time scale, the two trends were characterized by spike concentrations, due to freshly emitted vehicular exhausts. Due to the closer proximity to traffic, such spikes were more frequent and more intense at ground level than at

20 m heights. This circumstance made the road level aerosol concentrations on average richer in UFPs, particularly in nucleation mode particles. Hence, the aerosol infiltration efficiency was on average slightly higher at 20 m heights than at ground level. On the other hand, for the same reason, the road level aerosol concentration was on average more than double than at 20 m heights. As a result of that, the indoor aerosol concentration due to the penetration of outdoor particles was higher at ground floor than at 20 m height. With an estimated daily indoor permanence of 22 h, the daily dose deposited into the respiratory system was 3.55×10^{11} and 1.43×10^{11} particles, respectively, at ground level and at 20 m height. Such doses are greater than those estimated over the period of activity of some common combustion and non-combustion sources in indoor environments; therefore, they represent an important contribution to the total aerosol daily dose.

Supplementary Materials: The following are available online at <http://www.mdpi.com/2073-4433/10/12/772/s1>, Figure S1: Infiltration factors (F_{in}) estimated by interpolation of the average F_{in} measured by Bennett and Koutrakis [35], Figure S2: Atmospheric pressure, Temperature, Relative humidity, wind speed and wind direction throughout the aerosol measurements (averaging time 5 min).

Author Contributions: Conceptualization, M.M. and P.A.; methodology, M.M. and P.A.; software, M.M.; validation, M.M., C.P., M.V. and P.A.; formal analysis, M.M.; writing—original draft preparation, M.M. and C.P.; writing—review and editing, M.V. and P.A.

Funding: This research received no external funding.

Acknowledgments: The authors wish to thank ARA for MPPD Version 3.01. This study was carried out within the context of the Research Program 2019–2021 of National Institute for Insurance against Accidents at Work (INAIL).

Conflicts of Interest: The authors declare no conflict of interest.

Abbreviations

F_{in}	the particle infiltration factor
d_a	aerodynamic diameter
d_{ai}	aerodynamic diameter of the i^{th} aerosol size class
d_m	electrical mobility diameter
C_c	Cunningham slip factor
ρ_0	reference density (1 g cm^{-3})
ρ	particle density
χ	particle dynamic shape factor
H	head region of the respiratory system
TB	tracheobronchial region of the respiratory system
R	region of the respiratory system ($R = H, TB, Al$)
Al	alveolar region of the respiratory system
$F^R(d_{ai})$	particle regional deposition fractions per as a function of the aerodynamic diameter
V_t	tidal volume
C_{Tot}	Outdoor aerosol total number concentrations (1 s time resolution)
t	time
t_r	indoor residence time
t_{exp}	exposure time to outdoor aerosol and period of operation of indoor aerosol emission sources
t_{day}	daily time spent indoor
$C(d_{ai}, t)$	average aerosol concentration over a single inspiratory act as a function of time and of aerodynamic diameter
$D^R(d_{ai}, t)$	aerosol number doses deposited in the regions R of the respiratory system, as functions of time (t) and of the aerodynamic diameter

$D_{Tot}^R(t)$	total regional aerosol doses
$D_{Tot}^{Tot}(t)$	total aerosol doses deposited into the respiratory system
$D_{Tot}^R(t_r)$	cumulative regional doses over a given indoor residence time (t_r)
$D_{Tot}^{Tot}(t_r)$	cumulative total doses over a given indoor residence time
$D_{Tot}^R(t_{day})$	cumulative regional daily dose
$D_{Tot}^{Tot}(t_{day})$	cumulative total daily dose
$\dot{D}_{Tot}^{Tot}(t_{day})$	cumulative regional daily dose per unit time (t_{day})
$D_{Tot}^{Tot}(t_{exp})$	cumulative total doses over a given exposure time to outdoor aerosol or during the period of indoor emission sources operation
$\dot{D}_{Tot}^{Tot}(t_{exp})$	$D_{Tot}^{Tot}(t_{exp})$ per unit time (t_{exp})
$D_{Tot}^{Tot}(d_{ai}, t_r)$	cumulative total dose size distribution over a given indoor residence time
PBL	planetary boundary layer
GMD	geometric mean diameter
$F_{in}(GMD)$	1h mobile average infiltration factor calculated at the GMD

References

1. World Health Organization (WHO). Air Pollution. Available online: <https://www.who.int/airpollution/en/> (accessed on 18 September 2019).
2. Lehtomäki, H.; Korhonen, A.; Asikainen, A.; Karvosenoja, N.; Kupiainen, K.; Paunu, V.; Savolahti, M.; Sofiev, M.; Palamarchuk, Y.; Karppinen, A.; et al. Health Impacts of Ambient Air Pollution in Finland. *Int. J. Environ. Res. Public Health* **2018**, *15*, 736. [CrossRef] [PubMed]
3. Tang, C.S.; Wu, T.Y.; Chuang, K.J.; Chang, T.Y.; Chuang, H.C.; Candice Lung, S.; Chang, L.T. Impacts of In-Cabin Exposure to Size-Fractionated Particulate Matters and Carbon Monoxide on Changes in Heart Rate Variability for Healthy Public Transit Commuters. *Atmosphere* **2019**, *10*, 409. [CrossRef]
4. Wang, Y.; Xiong, L.; Tang, M. Toxicity of inhaled particulate matter on the central nervous system: Neuroinflammation, neuropsychological effects and neurodegenerative disease. *J. Appl. Toxicol.* **2017**, *37*, 644–667. [CrossRef] [PubMed]
5. International Agency for Research on Cancer (IARC). Monographs on the Evaluation of Carcinogenic Risks to Humans. International Agency for Research on Cancer. In *Outdoor Air Pollution*; WHO Press: Lyon, France, 2015; Volume 109. Available online: <http://monographs.iarc.fr/ENG/Monographs/vol109/index.php> (accessed on 10 September 2019).
6. Brauer, M.; Koutrakis, P.; Spengler, J.D. Personal exposures to acidic aerosols and gases. *Environ. Sci. Technol.* **1989**, *23*, 1408–1412. [CrossRef]
7. Isaxon, C.; Gudmundsson, C.; Nordin, E.Z.; Lönnblad, L.; Dahl, A.; Wieslander, G.; Bohgard, M.; Wierzbicka, A. Contribution of indoor-generated particles to residential exposure. *Atmos. Environ.* **2015**, *106*, 458–466. [CrossRef]
8. Heo, J.; Wu, B.; Abdeen, Z.; Qasrawi, R.; Sarnat, J.A.; Sharf, G.; Shpund, K.; Schauer, J.J. Source apportionments of ambient fine particulate matter in Israeli, Jordanian, and Palestinian cities. *Environ. Pollut.* **2017**, *225*, 1–11. [CrossRef]
9. Pagano, P.; De Zaiacomio, T.; Scarcella, E.; Bruni, S.; Calamosca, M. Mutagenic activity of total and particle-sized fractions of urban particulate matter. *Environ. Sci. Technol.* **1996**, *30*, 3512–3516. [CrossRef]
10. Li, N.; Sioutas, C.; Cho, A.; Schmitz, D.; Misra, C.; Sempf, J.; Wang, M.; Oberley, T.; Froines, J.; Nel, A. Ultrafine particulate pollutants induce oxidative stress and mitochondrial damage. *Environ. Health Perspect.* **2003**, *111*, 455–460. [CrossRef]
11. Chen, R.; Hu, B.; Liu, Y.; Xu, J.; Yang, G.; Xu, D.; Chen, C. Beyond PM_{2.5}: The role of ultrafine particles on adverse health effects of air pollution. *Biochim. Biophys. Acta* **2016**, *1860*, 2844–2855. [CrossRef]
12. Manigrasso, M.; Protano, C.; Vitali, M.; Avino, P. Where do Ultrafine Particles and Nano-Sized Particles come from? *J. Alzheimers Dis.* **2019**, *68*, 1371–1390. [CrossRef]
13. Da Costa, E.; Oliveira, J.R.; Base, L.H.; de Abreu, L.C.; Filho, C.F.; Ferreira, C.; Morawska, L. Ultrafine particles and children's health: Literature review. *Paediatr. Respir. Rev.* **2019**. [CrossRef]

14. Viitanen, A.-K.; Uuksulainen, S.; Koivisto, A.J.; Hämeri, K.; Kauppinen, T. Workplace measurements of ultrafine particles—A literature review. *Ann. Work Expo. Health* **2017**, *61*, 749–758. [[CrossRef](#)] [[PubMed](#)]
15. Avino, P.; Protano, C.; Vitali, M.; Manigrasso, M. Benchmark study on fine-mode aerosol in a big urban area and relevant doses deposited in the human respiratory tract. *Environ. Pollut.* **2016**, *216*, 530–537. [[CrossRef](#)] [[PubMed](#)]
16. Kangasniemi, O.; Kuuluvainen, H.; Heikkilä, J.; Pirjola, L.; Niemi, J.V.; Timonen, H.; Saarikoski, S.; Rönkkö, T.; Dal Maso, M. Dispersion of a Traffic Related Nanocluster Aerosol Near a Major Road. *Atmosphere* **2019**, *10*, 309. [[CrossRef](#)]
17. Manigrasso, M.; Vernale, C.; Avino, P. Traffic aerosol lobar doses deposited in the human respiratory system. *Environ. Sci. Pollut. Res. Int.* **2017**, *24*, 13866–13873. [[CrossRef](#)]
18. Manigrasso, M.; Natale, C.; Vitali, M.; Protano, C.; Avino, P. Pedestrians in traffic environments: Ultrafine particle respiratory doses. *Int. J. Environ. Res. Public Health* **2017**, *14*, 288. [[CrossRef](#)]
19. Rodríguez, S.; Van Dingenen, R.; Putaud, J.-P.; Dell’Acqua, A.; Pey, J.; Querol, X.; Alastuey, A.; Chenery, S.; Ho, K.-F.; Harrison, R.; et al. A study on the relationship between mass concentrations, chemistry and number size distribution of urban fine aerosols in Milan, Barcelona and London. *Atmos. Chem. Phys.* **2007**, *7*, 2217–2232. [[CrossRef](#)]
20. Buonanno, G.; Fuoco, F.C.; Stabile, L. Influential parameters on particle exposure of pedestrians in urban microenvironments. *Atmos. Environ.* **2011**, *45*, 1434–1443. [[CrossRef](#)]
21. Koivisto, A.J.; Jensen, A.C.Ø.; Kling, K.I.; Nørgaard, A.; Brinch, A.; Christensen, F.; Jensen, K. Quantitative material releases from products and articles containing manufactured nanomaterials: Towards a release library. *Nanoimpact* **2017**, *5*, 119–132. [[CrossRef](#)]
22. Manigrasso, M.; Vitali, M.; Protano, C.; Avino, P. Temporal evolution of ultrafine particles and of alveolar deposited surface area from main indoor combustion and non-combustion sources in a model room. *Sci. Total Environ.* **2017**, *598*, 1015–1026. [[CrossRef](#)]
23. Protano, C.; Manigrasso, M.; Avino, P.; Vitali, M. Second-hand smoke generated by combustion and electronic smoking devices used in real scenarios: Ultrafine particle pollution and age-related dose assessment. *Environ. Int.* **2017**, *107*, 190–195. [[CrossRef](#)] [[PubMed](#)]
24. Manigrasso, M.; Vitali, M.; Protano, C.; Avino, P. Ultrafine particles in domestic environments: Regional doses deposited in the human respiratory system. *Environ. Int.* **2018**, *118*, 134–145. [[CrossRef](#)] [[PubMed](#)]
25. Koivisto, A.J.; Kling, K.I.; Fonseca, A.S.; Bluhme, A.B.; Moreman, M.; Yu, M.; Costa, A.L.; Giovanni, B.; Ortelli, S.; Fransman, W.; et al. Dip coating of air purifier ceramic honeycombs with photocatalytic TiO₂ nanoparticles: A case study for occupational exposure. *Sci. Total Environ.* **2018**, *630*, 1283–1291. [[CrossRef](#)] [[PubMed](#)]
26. Manigrasso, M.; Protano, C.; Astolfi, M.L.; Massimi, L.; Avino, P.; Vitali, M.; Canepari, S. Evidences of copper nanoparticle exposure in indoor environments: Long-term assessment, high-resolution field emission scanning electron microscopy evaluation, in silico respiratory dosimetry study and possible health implications. *Sci. Total Environ.* **2019**, *653*, 1192–1203. [[CrossRef](#)] [[PubMed](#)]
27. Hubal, E.A.C.; Sheldon, L.S.; Burke, J.M.; McCurdy, T.R.; Berry, M.R.; Rigas, M.L.; Zartarian, V.G.; Freeman, N.C. Children’s exposure assessment: A review of factors influencing children’s exposure, and the data available to characterize and assess that exposure. *Environ. Health Perspect.* **2000**, *108*, 475–486. [[CrossRef](#)]
28. Morawska, L.; Ayoko, G.A.; Bae, G.N.; Buonanno, G.; Chao, C.Y.H.; Clifford, S.; Fu, S.C.; Hänninen, O.; He, C.; Isaxon, C.; et al. Airborne particles in indoor environment of homes, schools, offices and aged care facilities: The main routes of exposure. *Environ. Int.* **2017**, *108*, 75–83. [[CrossRef](#)]
29. Śmiełowska, M.; Marć, M.; Zabiegała, B. Indoor air quality in public utility environments—a review. *Environ. Sci. Pollut. Res.* **2017**, *24*, 11166–11176. [[CrossRef](#)]
30. Quang, T.N.; He, C.; Morawska, L.; Knibbs, L.D.; Falk, M. Vertical particle concentration profiles around urban office buildings. *Atmos. Chem. Phys.* **2012**, *12*, 5017–5030. [[CrossRef](#)]
31. Goel, A.; Kumar, P. Vertical and horizontal variability in airborne nanoparticles and their exposure around signalised traffic intersections. *Environ. Pollut.* **2016**, *214*, 54–69. [[CrossRef](#)]
32. Kuuluvainen, H.; Poikkimäki, M.; Järvinen, A.; Kuula, J.; Irjala, M.; Dal Maso, M.; Keskinen, J.; Timonen, H.; Niemi, J.V.; Rönkkö, T. Vertical profiles of lung deposited surface area concentration of particulate matter measured with a drone in a street canyon. *Environ. Pollut.* **2018**, *241*, 96–105. [[CrossRef](#)]

33. TSI Particle Technology. 2009. Available online: https://www.tsi.com/mwg-internal/de5fs23hu73ds/progress?id=RIM4jnSl3c1lzZ_fGE6mizpum3DwsAGjm7nr4S7XilQ,&dl (accessed on 10 September 2019).
34. Jeong, C.-H.; Greg, J.; Evans, G.J. Inter-comparison of a fast mobility particle sizer and a scanning mobility particle sizer incorporating an ultrafine water based condensation particle counter. *Aerosol Sci. Technol.* **2009**, *43*, 364–373. [\[CrossRef\]](#)
35. Bennett, D.H.; Koutrakis, P. Determining the infiltration of outdoor particles in the indoor environment using a dynamic model. *Aerosol Sci.* **2006**, *37*, 766–785. [\[CrossRef\]](#)
36. De Boor, C. *A Practical Guide to Splines*; Springer: New York, NY, USA, 1978.
37. Hussein, T.; Löndahl, J.; Paasonen, P.; Koivisto, A.J.; Petäjä, T.; Hämeri, K.; Kulmala, M. Modeling regional deposited dose of submicron aerosol particles. *Sci. Total Environ.* **2013**, *458*, 140–149. [\[CrossRef\]](#) [\[PubMed\]](#)
38. Asgharian, B.; Hofmann, W.; Bergmann, R. Particle deposition in a multiple-path model of the human lung. *Aerosol Sci. Technol.* **2001**, *34*, 332–339. [\[CrossRef\]](#)
39. International Commission on Radiological Protection (ICRP). *Publication 66: Human Respiratory Tract Model for Radiological Protection*; Elsevier Science: Oxford, UK, 1994.
40. Hussein, T.; Saleh, S.S.A.; dos Santos, V.N.; Boor, B.E.; Koivisto, A.J.; Löndahl, J. Regional Inhaled Deposited Dose of Urban Aerosols in an Eastern Mediterranean City. *Atmosphere* **2019**, *10*, 530. [\[CrossRef\]](#)
41. Khlystov, A.; Stanier, C.; Pandis, S.N. An algorithm for combining electrical mobility and aerodynamic size distributions data when measuring ambient aerosol special issue of aerosol science and technology on findings from the fine particulate matter supersites program. *Aerosol Sci. Technol.* **2004**, *38*, 229–238. [\[CrossRef\]](#)
42. Lipponen, P.; Hänninen, O.; Sorjamaa, R.; Gherardi, M.; Gatto, M.P.; Gordiani, A.; Cecinato, A.; Romagnoli, P.; Gariazzo, C. *Aerosol Processes in PAH Infiltration and Population Exposure in Rome*; EAC: Prague, Czech Republic, 2013. Available online: [https://appsricercascientifica.inail.it/expah/documenti/Lipponen%20et%20al.2013.EAC%20Prague%20on%20EXPAH%20Slides\(v5\).pdf](https://appsricercascientifica.inail.it/expah/documenti/Lipponen%20et%20al.2013.EAC%20Prague%20on%20EXPAH%20Slides(v5).pdf) (accessed on 23 September 2019).
43. Hänninen, O.; Sorjamaa, R.; Lipponen, P.; Cyrus, J.; Lanki, T.; Pekkanen, J. Aerosol-based modelling of infiltration of ambient PM_{2.5} and evaluation against population-based measurements in homes in Helsinki, Finland. *J. Aerosol Sci.* **2013**, *66*, 111–122. [\[CrossRef\]](#)
44. Hu, M.; Peng, J.; Sun, K.; Yue, D.; Guo, S.; Wiedensohler, A.; Wu, Z. Estimation of size-resolved ambient particle density based on the measurement of aerosol number, mass, and chemical size distributions in the winter in Beijing. *Environ. Sci. Technol.* **2012**, *46*, 9941–9947. [\[CrossRef\]](#)
45. Perrino, C.; Pietrodangelo, A.; Febo, A. An atmospheric stability index based on radon progeny measurements for the evaluation of primary urban pollution. *Atmos. Environ.* **2001**, *35*, 5235–5244. [\[CrossRef\]](#)
46. Avino, P.; Manigrasso, M. Dynamic of submicrometer particles in urban environment. *Environ. Sci. Pollut. Res. Int.* **2017**, *24*, 13908–13920. [\[CrossRef\]](#)
47. Manigrasso, M.; Febo, A.; Guglielmi, F.; Ciambottini, V.; Avino, P. Relevance of aerosol size spectrum analysis as support to qualitative source apportionment studies. *Environ. Pollut.* **2012**, *170*, 43–51. [\[CrossRef\]](#) [\[PubMed\]](#)
48. Zhang, L.; Gong, S.; Padro, J.; Barrie, L. A size-segregated particle dry deposition scheme for an atmospheric aerosol module. *Atmos. Environ.* **2001**, *35*, 549–560. [\[CrossRef\]](#)
49. Chen, C.; Zhao, B. Review of relationship between indoor and outdoor particles: I/O ratio, infiltration factor and penetration factor. *Atmos. Environ.* **2011**, *45*, 275–288. [\[CrossRef\]](#)
50. Manigrasso, M.; Protano, C.; Martellucci, S.; Mattei, V.; Vitali, M.; Avino, P. Evaluation of the Submicron Particles distribution between mountain and urban site: Contribution of the transportation for defining environmental and human health issues. *Int. J. Environ. Res. Public Health* **2019**, *16*, 1339. [\[CrossRef\]](#) [\[PubMed\]](#)

